# A preliminary investigation of a novel mortar based on alkali-activated seashell waste powder

Abdelaziz Hasnaoui, Amel Bourguiba, Yassine El Mendili, Nassim Sebaibi, Mohamed Boutouil

# A preliminary investigation of a novel mortar based on alkali-activated seashell waste powder

Abdelaziz HASNAOUI[*,1], Amel BOURGUIBA[1], Yassine El MENDILI[1], Nassim SEBAIBI[1], Mohamed BOUTOUIL[1].

## Abstract

This paper presents the preliminary findings on a new mortar prepared with alkali-activated seashell waste (AASW). Three mortars were manufactured with seashell waste to Activator ratios of 2.5, 3 and 3.5. The mechanical properties were determined, and the chemical products of each mixture were characterized using TG/DTG, XRD and FTIR analyses. From both an economic and an environmental point of view, the obtained results are very encouraging where they show that SW can be used as precursor to formulate an alkali-activated mortar with a compressive strength of 22 MPa and a porosity of 16.5%. The AASW paste was found to be mainly composed of C-S-H and different carbonates such as gaylussite, pirssonite and thermonatrite. In terms of mechanical strengths and porosity, it was established that the water to biner ratio is the key factor. Furthermore, the microstructural images showed a good compatibility between the AASW paste and aggregates.

**Keywords:** Environmental impact; Alkali-activated materials; Mortar; Seashell waste powder; Carbonates.

[*] Corresponding author: abdelaziz.hasnaoui@esitc-caen.fr . Tel: +33647076181.
1- Laboratoire de Recherche ESITC Caen, ComUE Normandie Université, 1 Rue Pierre et Marie Curie, 14610, Epron, France.

## 1. Introduction

Today, there is no doubt that the humanity is in deep trouble due the current climate and environmental crises. Indeed, the gravity of the situation has prompted more than 11,000 scientists around the globe to declare, clearly and unequivocally, that our planet is facing a climate emergency [1]–[3]. Henceforth, dealing with this catastrophic threat is no longer an option, but an urgent necessity that requires the improvement of the resource efficiency policies adopted by all the involved actors, including the construction industry, in order to create a more sustainable economy and preserve our planet. This cannot be achieved without the development of new low-carbon building materials to avoid the environmental impacts of the cement industry.

It is well known that concrete and mortars are one of the keystones of our modern infrastructure. However, over the last few decades, environmental degradation due to ordinary Portland cement (OPC) manufacturing has gone up at an alarming rate [4]. In fact, OPC industry generates around 7% of the annual worldwide anthropogenic $CO_2$ emissions in addition to the large amount of nitrogen oxide, sulfur oxide and particulate matter smaller than 10 microns [4], [5]. Despite the contribution of OPC-based materials carbonation to sequestrating part of the earth's $CO_2$ [6], the remain emissions, including the other toxic gases, contribute significantly to the environmental degradation.

In addition to this serious problem, the overexploitation of non-renewable raw materials for OPC production gives rise to another set of environmental issues [7]. Faced with this global concern, considerable efforts have been made to limit the $CO_2$ footprint of OPC-based materials and preserve the natural non-renewable resources of our planet. These efforts consist mainly in either substituting OPC by different supplementary cementing materials or developing clinker free cements [8]–[10]. In this context, alkali-activated materials (AAM) have been widely proposed as a viable alternative to OPC [11]–[13]. They are obtained

through the activation of an aluminosilicate raw materials using an alkaline solution [14]. The chemical structure of AAM depends primarily on the presence of calcium in the precursor. In fact, the activation of a calcium-rich raw materials such as slag results in chemical system mainly based on calcium alumina silicate hydrate (C–A–S–H) gel with a tobermorite-like structure, while the alkali activation of low-calcium materials such as class F fly ash or pure calcined clays generates a sodium alumina silicate hydrate (N–A–S–H) gel with a highly crosslinked and disordered pseudo-zeolitic structure [15]. The most aluminosilicate precursors used for AAM formulation are generally fly-ash, slag and metakaolin [16]. Using these materials in AAM preparation can actually lead to a relative $CO_2$ footprint reduction which vary largely from a formulation to another, depending on the type, the source and the dosage of the raw materials and the alkali activators [17], [18]. However, despite the environmental benefit of fly-ash, slag and metakaolin alkali activation, these commonly used aluminosilicate materials are not available all over the world, which led scientists to pursue the search for the activation of more sustainable and widely available raw materials, such as limestone.

In general, a positive effect was reported when limestone or other carbonate fines were added as partial replacement of fly ash, slag or metakaolin to prepare AAM, by enhancing the mechanical performances, decreasing the porosity and limiting shrinkage [19]. Indeed, when limestone was added as partial replacement of metakaolin, the optimal AAM paste in terms of mechanical strength was obtained with 32.32 % of limestone [20]. However, in terms of alkali activation of limestone as only precursor, only few studies are available in the literature with relatively few details [21]–[23]. In this respect, Ortega-Zavala *et al.* [21] have studied the activation of limestone using a mix of commercial sodium silicate and sodium hydroxide. They have shown that limestone can be used as a precursor to produce AAM with compressive strengths ranging from 15 to 25 MPa after 360 days [21]. The reaction products in the obtained system was found to be a mixture of silica gel, calcium silicate hydrate (C-S-

74 H), sodium calcium silicate hydrate (N-C-S-H), sodium silicate gel (N-S-H) and crystalline
75 phases such as thermonatrite and pirssonite [21].
76 The use of limestone as the only precursor for AAM formulation reduces considerably the
77 $CO_2$ emissions and the energy requirements [21], nonetheless, both the environmental impact
78 and the economic costs could be more limited by using a waste product rather than limestone.
79 Such seems to be the case of seashell waste which is similar to limestone since its main
80 component is calcium carbonate ($CaCO_3$) [24].
81 Seashell waste is considered as a fishery industry by-product and many countries worldwide
82 are suffering from millions of tonnes of it, where its management is becoming increasingly
83 difficult [25]. Indeed, while only few amounts of seashell waste are re-used as fertilizers and
84 handicrafts, most of this waste ends up being landfilled without any treatment. This results in
85 foul odors due to the decay of the remaining flesh in the shells and the microbial
86 decomposition of salts into toxic gases such as hydrogen sulfide and ammonia [26]. In aiming
87 to valorize seashell waste in construction materials field, several investigations have been
88 devoted to studying the feasibility of incorporating this waste in mortars and concrete either
89 as aggregates or as additive powder for partial substitution of OPC [27]–[29], but the
90 activation of seashell waste powder to prepare a green binder has not been addressed
91 previously in the literature. Therefore, this paper presents the first results on the alkali
92 activation of seashell waste to formulate an alkali-activated mortar.
93
94

## 2. Materials and methods

### 2. 1 Materials

#### 2.1.1. Seashell waste

The seashell waste (SW) used in the present investigation is the queen scallop shells. They were provided in aggregate form by the suppliers of sea products of the north-west of France. The seashells were cleaned and dried at 40 °C during 24 hours to eliminate all visual flesh traces and impurities before being crushed with a drum compactor. In order to obtain SW powder, the received SW aggregates were crushed again by the Los Angeles abrasion machine and sieved through 63 microns sieve (**Fig. 1**). The obtained SW powder is characterized by a density of 2635 kg/m$^3$ and a specific surface area (Blaine) of 0.43 m$^2$/g. Using a laser diffraction particle size analyzer, its $d_{10}$, $d_{50}$, and $d_{90}$ were found to be 2.88, 23.38 and 49.48 μm, respectively (**Fig. 2(a)**). As it can be seen in the image from optical microscope (**Fig. 2(b)**), SW powder is a mix of an irregularly platy shaped particles. The slender of the platy particles is due to the thin layered structure of seashells.

The thermal gravimetric analysis (TG/DTG) results presented in **Fig. 3** indicate that SW powder is mainly composed of naturally precipitated calcium carbonate ($CaCO_3$). This is confirmed by the chemical composition listed in **Table 1**, and the X-ray diffraction (XRD) pattern illustrated in **Fig. 4**. Furthermore, the XRD results show that the crystalline form of $CaCO_3$ in SW powder consists primarily of calcite (94.8 % by volume) with 5 % of aragonite and some traces of vaterite (0.2 %).

#### 2.1.1. Alkaline solution

Sodium silicate solution (SS) with molar ratio (MR) $SiO_2/Na_2O$ of 2.1 was used to prepare the alkali-activated SW pastes and mortars. The chemical composition of SS is depicted in **Table 2**.

#### 2.1.1. Aggregate

The aggregate used for mortars formulation is a natural river sand (0-4 mm) with a fineness modulus of 2.7 and a density of 2750 kg/m$^3$.

### 2. 2. Formulation and curing modality

It is commonly known that the alkaline solution percentage plays a crucial role on the rheological and the mechanical properties of AAM. In fact, the whole process of the alkali activation depends on the alkaline solution content which affects the dominant factors influencing the performance of AAM, such as the alkali salts percentage and the water to binder ratio (w/b). For this raison, it was decided, as a preliminary study, to optimize the alkaline solution content for AASW mortars formulation by varying the SW to Activator (SW / dry extract of SS) and w/b ratios with keeping both the molar ratio $SiO_2/Na_2O$ of the alkaline solution and the SW powder finesses constant.

To this end, three AASW mortars, named M 2.5, M 3 and M 3.5, were prepared with a SW/Activator ratio of 2.5, 3 and 3.5, respectively. The SW powder weight (450 g) as well as the molar ratio $SiO_2/Na_2O$ of the alkaline solution (MR of 2.1) and the aggregate weight (1350 g) were kept constant for the three mixtures (**Table 3**). In addition to the mortars, simples of AASW pastes, named P 2.5, P 3 and P 3.5 were also prepared with the same paste formulation of M 2.5, M 3 and M 3.5, respectively. The pastes were characterized by the X-

ray diffraction (XRD), the thermogravimetric (TG/DTG) and the Fourier-transform infrared spectroscopy (FTIR) analyses. The mixing process of mortars was done in 5 minutes through two phases: (1) Mixing the SW powder and SS in the mixer during 1 minute at low rotation speed followed by 1 minute at high rotation speed; (2) Adding the sand to the paste and mixing for 1 minute at low rotation speed followed by an additional 2 minutes at high rotation speed. The mortars were then cast into standardized 4×4×16 mm moulds and compacted with 60 jolts using a jolting apparatus. Afterwards, they were placed in a ventilated oven for 48 hours at 60°C. After demoulding, the mortars were stored in a controlled hygrothermal room at $23^{\pm 2}$ °C and $50^{\pm 5}$ % RH (Relative humidity).

On the other hand, pastes preparation was also carried out in 5 minutes using 1 minute of low-speed mixing and 4 minutes of high-speed mixing. The paste simples were cast into plastic cylinder moulds of 3 cm diameter and 6 cm height. The same curing protocol adopted for mortars was identically applied for pastes.

### 2. 3 Characterization methods

At the fresh state, the workability of mortars was assessed using a flow table test according to the ASTM standard C230 / C230M – 08. At the hardened state, the compressive and flexural strengths of AASW mortars were tested after 3, 14 and 28 days of curing. The mechanical tests were carried out with an automatic hydraulic press machine at a loading rate of 2.4 kN/s and 0.05 kN/s for compressive and flexural strengths, respectively. The apparent density and the water porosity of mortars at 28 days were determined using the vacuum saturation method in accordance with NF P 18-459. As mentioned above, XRD analysis as well as TG/DTG and FTIR tests were conducted on AASW pastes to characterize the reaction products of the binder activation. Hence, AASW pastes were crushed at 28 days into fine powders by a planetary ball mill (Retsch™ PM 400 Model) before being tested. The FTIR test was carried

165 out via a Bruker Tensor 27 FT-IR equipment where infrared spectrums were recorded
166 between 600 and 4000 $cm^{-1}$. TG analysis of both SW powder and AASW pastes was
167 performed with NETZSCH instrument (STA 449 F5 Jupiter). The heating rate was fixed at
168 5°C $min^{-1}$ and the obtained data were analyzed by NETZSCH Proteus software.
169 XRD measurements were performed at room temperature with a D8 Advance Vario 1 Bruker
170 (A two-circle diffractometer, θ-2θ Bragg-Brentano mode), equipped with a Ge (111)
171 monochromator to obtain a monochromatic Cu Kα radiation (λ = 1.54059 Å). XRD data were
172 recorded for 2θ varying from 15° to 80° for 2 sec per 0.01° step (4 h/scan). NIST SRM-660b
173 $LaB_6$ standard powder (NIST SRM-660b) was used to calibrate the instrument [30]. Phase
174 identification were carried out using the Crystallography Open Database [31] and MAUD
175 software [32] was used for the Rietveld quantitative analysis.
176

177 **3. Results and discussion**

178 **3. 1 Mechanical strengths**

179 The compressive and flexural strengths of the three AASW mortars at 3, 14 and 28 days are
180 shown in **Fig. 5**. As expected, the effect of SS percentage was found to be significant on the
181 mechanical performance of mortars. However, while the best mechanical strengths were
182 anticipated for mortar with the highest Activator content (M 2.5), the opposite was the case.
183 In fact, the false anticipation assumed that the effect of the Activator content is more crucial
184 than that of w/b when the latter is in the range of 0.36 and 0.46, but the experimental results
185 showed the opposite pattern.

186 The recorded compressive strengths of M 2.5, M 3 and M 3.5 at 28 days were 14.9, 17.8 and
187 22.2 MPa; while their flexural strengths were 4.5, 5.2 and 5.5 MPa respectively. Since the
188 activated precursor consists of only SW waste powder, the obtained mechanical strengths can
189 be considered as promising results, especially those obtained for M 3.5. As a comparison, the

compressive strength achieved for M 3.5 is higher than that reported for alkali activated limestone-based mortars in previous study, which was around 19 MPa [21]. Furthermore, this strength was obtained after 360 days; while the best results at 1, 14 and 28 days were up to 8 MPa [21]. Given that the reported alkali activated limestone-based mortars were cured at 60°C for 24 hours, the relatively high compressive strengths obtained at early age in the present study suggests that extending the heat curing to 48 hours should be very beneficial regarding the early age mechanical properties. This is in agreement with the observation reported by Perez-Cortez *et al.* [20], where it was found that heat curing of alkali activated metakaolin-limestone mix at 60°C for 24 h was insufficient to complete the reaction process.

The lowest mechanical results at 3, 14 and 28 days were obtained for M 2.5 which is prepared with the highest SS content and consequently, the highest w/b ratio (0.46). In addition, a proportional decrease in mechanical properties with increasing SS percentage (decreasing SW/Activator) was recorded. This may be due in part to the fact that high w/b ratio contributes to increasing the mortar porosity via the evaporation of the free water during the whole curing period. The proposed interpretation can be supported by the water porosity results discussed later. **Fig. 6** Shows the failure mode of AASW mortars under uniaxial compression test at 28 days. The obtained failure pattern for the three mortars is a semi-explosive mode with little damage to compression faces. This satisfactory failure is commonly observed for conventional mortars, and it confirms the compression test reliability and the homogenous structure of the AASW mortars.

A similar evolution kinetic with an enhancement trend over time for both compressive and flexural strengths was obtained for the three AASW mortars. The strength increasing over time is due to the evolving pattern of the alkali activation reactions, and it is a positive indicator of SW powder reactivity. Indeed, the strength gains are obviously the result of chemical products formation which begins with the dissolution of the calcite ($CaCO_3$) from

SW powder to give place to $Ca^{2+}$ ions. These latter, in presence of a saturated $CO_2$ and sodium silicate medium, promotes the formation of hydrate gels and crystalline phases [22]. As reported in previous studies where calcite-rich powder was included in the alkali activation process, the formation of these chemical products leads to the mechanical strength gain over time [20]–[22]. The formation and the identification of the involved chemical products will be described later in the section devoted to AASW paste characterization.

### 3. 2 Water porosity and apparent density

The apparent density and the water porosity results of M 2.5, M 3 and M 3.5 are presented in **Fig. 7**. As it can be seen, AASW mortars showed an apparent density up to 2 g/cm$^3$ and a proportional increase with respect to the SW/Activator ratio was recorded. It is worth noting that the low density of AASW mortars compared to conventional OPC or geopolymer-based mortars is the results of the low density of SW powder [16]. In the other hand, the water porosity values were found to range between 16.5 and 22.3% but rather with a decreasing trend with the augmentation of SW/Activator ratio. These results are fully consistent with the obtained mechanical performances, where the highest mechanical strengths were recorded for mortars with the lowest porosity and vice versa. In order to clarify the effect of the alkaline solution amount in the porosity of AASW mortars, the water porosity values versus w/b ratio are illustrated in **Fig. 8**. Obviously, a strong linear relationship can be observed which confirms the mechanical results interpretations advanced previously. Indeed, the alkaline solution excess in the mixture implies an increase in the free water evaporation during curing which promotes the formation of micro-cracks in AASW matrix and results in more porous structure, and consequently, lowest strengths. This explanation is supported by the microscopic images (**Fig. 9**) of the AASW mortar where the presence of micro-cracks in the AASW matrix were observed even with the optimal mixture (M 3.5). The microscopic images

also reveal a crucial detail regarding the compatibility between the AASW binder and the natural river sand. In fact, a good adhesion between the two phases can be seen in the images which explains in part the promising strengths obtained for this new mortar. It should be noted that no visual sign of degradation or efflorescence formation was observed in the surface of the mortars, which is a positive indicator in terms of the physical stability of AASW mortars.

## 3. 3 Characterization of the reaction products

### 3.3.3. TG/DTG analysis

**Fig. 10**. displays the TG/DTG curves of AASW pastes and SW powder. In each graph, the results of AASW pastes were presented with those of SW powder in order to provide a clear vision on the precursor transformation through the alkali activation process. From these graphs, it can be noticed that the three AASW pastes show a first mass decline between 20 and 200°C which is reflected in a DTG peak at around 110°C. This mass loss corresponds to three phenomena that can take place in the temperature range of 20-200°C: (1) the evaporation of free water in the mix; (2) the dehydration of hydrates gels such as C-S-H, N-S-H and N-C-S-H, that usually emerge in alkali-activated rich-calcite systems [21] ; (3) the dehydration of the formed carbonates such as gaylussite and pirssonite [22].

The specific DTG peak of C-S-H dehydration, reported generally in OPC-based materials and AAM at a temperature of 75-95°C, was not observed separately in our study [33], [34]. This is due to the dominant peak of free water evaporation in one hand and the relatively low amount of C-S-H in the AASW systems in the other hand. Nevertheless, the presence of C-S-H phases was revealed by the FTIR spectroscopy analysis that will be discussed later. It is noteworthy that the slight difference in the rate of the first mass loss is in accordance with the

SW/Activator ratio (SS percentage) of the AASW pastes, where the highest mass loss is attributed to P 2.5 while the lowest one was recorded for P 3.5. These results confirm once again the presence of more free water in M 2.5.

At around 500°C, a second mass loss was occurred for all AASW pastes, with a DTG peak at 715°C. Then, a third mass loss was recorded in the temperature range of 750-800°C, corresponding to a DTG peak at 770°C. The emergence of these two DTG peaks is solid proof of the SW powder reactivity. Indeed, the peak at 770°C is due to the decarbonation of unreacted $CaCO_3$ originating from SW powder; but the one at around 715°C is attributed to the decomposition and melting of $Na_2Ca(CO_3)_2$. These double carbonates ($Na_2Ca(CO_3)_2$) are the result of the dehydration of the precipitated carbonates (gaylussite and pirssonite) formed from $CaCO_3$ reaction with the alkaline solution. The thermal dehydration and decomposition of gaylussite and pirssonite can be summarized as follows [22], [35], [36]:

(1) Gaylussite:

$$Na_2Ca(CO_3)_2.5H_2O \xrightarrow{125°C} Na_2Ca(CO_3)_2 + 5H_2O$$

$$Na_2Ca(CO_3) \xrightarrow{715°C} Na_2CO_3 + CaO + CO_2 \uparrow$$

(2) Pirssonite:

$$Na_2Ca(CO_3)_2.2H_2O \xrightarrow{175°C} Na_2Ca(CO_3)_2 + 2H_2O$$

$$Na_2Ca(CO_3) \xrightarrow{715°C} Na_2CO_3 + CaO + CO_2 \uparrow$$

Furthermore, a remarkable shift of the calcite decomposition peak from 850°C (in powder form) to 770°C (in activated form) was observed for all AASW mixtures. The observed behavior is in good agreement with the findings of Malik *et al.* [37] which showed that the decomposition temperature of $CaCO_3$ tends to decrease in the presence of alkaline salts. Similar conclusions were also reported by Anbalagan *et al.* [38] and Avila-López *et al.* [22].

At around 850°C, a fourth DTG peak was only detected for P 2.5 sample that is prepared with the highest SS content. The mass loss corresponding to this peak was far lower than those of carbonates (around 2%). The emergence of this peak in only P 2.5 indicates that the considerable amount of unreacted SS in the mixture is the cause of this fourth mass loss. In fact, this peak may be due to the decomposition of crystalline products formed from the amorphous SS during heat curing. In a published study on the phase evolution of sodium silicate solution under heat treatment [39], it was found that heating the amorphous sodium silicate gives rise to the formation of cristobalite [39]. In addition, Bloise *et al.*[40] found that the collapse cristobalite structure occurs at 850°C, which is the temperature at which the fourth peak in P 2.5 sample is observed. This interpretation regarding the emergence of the fourth peak is evidenced by the X ray diffraction results presented in the next section, where the presence of cristobalite phase in P 2.5 was revealed.

### 3.3.3. XRD analysis and FTIR spectroscopy

The XRD diffractograms of P 2.5, P 3 and P 3.5 at 28 days are presented in **Fig. 11**. The calculated pattern (red line) is superimposed on the observed profile (coarse line) while the difference curve ($I_{obs}$-$I_{calc}$) is shown at the bottom of the figure. The general agreement R-factors are up to 10%, which indicates a high goodness of fit between the model and the experimental data.

The XRD patterns reveal that the crystalline products in the AASW systems consist in gaylussite ($Na_2O(CO_3)_2(H_2O)_5$), pirssonite ($Na_2O(CO_3)_2(H_2O)_5$), portlandite ($Ca(OH)_2$) and thermonatrite ($Na_2O(CO_3)_2H_2O$. For the three mixtures, Gaylussite was found to be the dominant crystalline phase with a volumetric percentage of 55.3, 38.3 and 66.4% for P 2.5, P 3 and P 3.5, respectively; while the percentages of thermonatrite in the pastes were up to 3.5%

312 regardless the SW/Activator ratio. As regard the portlandite formation, its presence in P 2.5
313 was relatively high (6.9%) in comparison with the traces detected for P 3 and P 3.5 (0.3%).
314 This result suggests that the high water content in P 2.5 mixture may favorize the formation of
315 portlandite. Ortega-Zavala *et al.* [21] suggested that the formation of carbonates can decrease
316 the porosity of the alkali activated limestone pastes, which results in a dense matrix and,
317 consequently, a higher compressive strength. This seems to be the case in the present study
318 given the promising performances obtained for AASW mortars, especially those of M 3.5.
319 Considering the TG/DTG results of P 2.5, which revealed the formation of cristobalite from
320 the excess of amorphous SS, the XRD pattern of P 2.5 confirms the presence of this
321 crystalline silicon dioxide phase. Indeed, eminent reflections of cristobalite was observed only
322 in P 2.5. It is important to point out that the obtained low percentage of cristobalite is
323 consistent with the mass loss recorded in the TG test.

324 As shown above in TG/DTG curves, a portion of calcite and aragonite remained unreacted
325 after activation, and their overshadowing intense reflections remained in the XRD
326 diffractograms of AASW pastes. However, the comparison between the crystalline structure
327 of the calcite in SW powder and that in AASW pastes reveals that the unreacted calcite in the
328 activated system was not completely unaffected by the alkaline solution (**Fig. 12**). The
329 adopted technique for the assessment of the crystalline structure of $CaCO_3$ consists in using a
330 harmonic texture model (included in the Rietveld fit) with a fiber component as implemented
331 in Maud. This allows to accurately reproduce the diffracted intensities of the calcite in both
332 SW powder and AASW pastes. It is noteworthy that the refined textures presented in **Fig. 12**
333 correspond to $\vec{c}$ axes perpendicular to the sample plane, with the $\vec{a}/\vec{b}$ axes at random around
334 c, i.e. c <006> fiber texture component.

335 As it can be seen in the presented calcite pole figures, the maximum orientation density of the
336 {006} pole figure was found to be around 2.1 m.r.d for SW powder while a lower maximum

orientation densities were recorded for AASW pastes (around 1.2 and 1.3 m.r.d). The decrease of texture strength of calcite in the AASW pastes compared to SW powder is due to the effect of the alkaline solution in the ductility of the $CaCO_3$ crystals which lead to the increase of calcium dissolution and/or decomposition. This adequately explains the shift of the DTG peak of the calcite decomposition observed above and confirms that the decomposition temperature of calcite tends to decrease in alkaline medium.

The intense reflections of calcite and the low crystallinity of C-S-H have both prevented the detection of C-S-H in the XRD diffractograms. Nevertheless, the formation of C-S-H in AASW systems was revealed with the FTIR spectroscopy results, presented in **Fig. 13** and **Table 4**. As it can be seen in the displayed FTIR spectrum, AASW pastes exhibit an absorption band at about 981 $cm^{-1}$ which is attributed the to the stretching vibrations in Si-O bonds in $Q^2$ tetrahedra of the C-S-H gel [21], [41]–[43]. In addition, the band at 2504 $cm^{-1}$, observed in SW powder spectrum, was not detected in AASW pastes. This band is commonly observed in the bivalve shells such as mussel, oyster and scallop shells, and it corresponds to the harmonic vibration in $2\nu_2 + \nu_4$, C-O bonds [44]. The absence of this band in the activated mixtures reveals the dissolution of $CaCO_3$ to form C-S-H and carbonates.

The bands initially observed in SW powder spectra at 712, 864, 1392 and 1412 $cm^{-1}$ were found to persist in the AASW mixtures with only slightly shift in wavenumbers (between 8 and 12 $cm^{-1}$). These bands are typical characteristics of $(CO_3)^{2-}$ functional group of both the SW powder and the formed new carbonates in the activated systems [43]–[47], and their persistence is in good agreement with the TG/DTG and the XRD results. Moreover, the slight shift of these bands in the AASW pastes can be explained by the structural transformation of the unreacted $CaCO_3$ in presence of alkalis as discussed above as well as the formation of new carbonates.

At 667 $cm^{-1}$ and 2343 $cm^{-1}$, low-intensity bands were detected in the three pastes. The first band (667 $cm^{-1}$) is assigned to the bending vibrations in Si-O-Si bonds which indicates the formation of silica gel via the condensation of the unreacted SS [21]; while the band at 2343 $cm^{-1}$ is attributed to the $\nu_3$ C-O asymmetric stretching mode in $CO_2$ molecule [48], [49]. The presence of carbon dioxide in the pastes was promoted by their relatively high porosity which allows $CO_2$ to be more readily absorbed.

## 4. Concluding remarks and future perspectives

This paper presents the first results obtained on alkali-activated mortars based on seashell waste as precursor. The physical and the mechanical characterizations of the prepared mortars as well as the analysis of the emerged chemical products have yielded some promising findings which are summarized as follows:

- Calcite-rich SW can be valorized as a precursor for the preparation of alkali-activated mortar with a compressive strength of 22 MPa at 28 days.
- The mechanical properties and the porosity of AASW mortars were dominated by the w/b ratio rather than by the activator content.
- The activation of SW by a sodium silicate solution with a molar ratio $SiO_2/Na_2O$ of 2.1 results in AASW matrix composed by a mix of unreacted SW particles as well as gaylussite, pirssonite, thermonatrite, portlandite and C-S-H.
- The type and the proportion of the formed chemical products in AASW depend on the SS percentage in the mix. Furthermore, an excess of SS in the mix favorizes the formation of cristobalite crystals.
- The TG/DTG results, and those of XRD and FTIR analyses provided solid proof of the SW alkali-reactivity and they led to explain the decrease of $CaCO_3$ decomposition temperature in presence of alkalis.

- In terms of mechanical strengths and water porosity, the optimal AASW mortar was achieved with MR of 2.1, SW/Activator of 3.5 and w/b of 0.36.
- The microstructural images of the optimal mortar revealed a good compatibility between the AASW paste and the natural river sand, and no visual sign of degradation or efflorescence formation was observed in the surface of the mortars.

With a compressive strength of 22 MPa at 28 days, and around 16 % of porosity, the AASW mortar proposed in the present work can be considered as a cost effective and sustainable building material. Moreover, it seems to be able to cover a large range of applications in civil engineering industry. Nevertheless, this study should be supplemented by further investigations such as the effect of the curing modality, the finesses of the SW powder and the type of activator on the performance of AASW binder. Investigations on the durability of this type of mortars are also required to establish a real alternative to conventional mortars.

## References


[1] W. Ripple, C. Wolf, T. Newsome, P. Barnard, W. Moomaw, and P. Grandcolas, "World scientists' warning of a climate emergency," *Bioscience*, 2019.

[2] R. Pierrehumbert, "There is no Plan B for dealing with the climate crisis," *Bull. At. Sci.*, vol. 75, no. 5, pp. 215–221, 2019.

[3] V. Galaz, "Climate and Environmental Crises," in *Oxford Research Encyclopedia of Politics*, 2020.

[4] S. A. Miller and F. C. Moore, "Climate and health damages from global concrete production," *Nat. Clim. Chang.*, pp. 1–5, 2020.

[5] N. B. Singh and B. Middendorf, "Geopolymers as an alternative to Portland cement:

410 An overview," *Constr. Build. Mater.*, vol. 237, p. 117455, 2020.

411 [6] F. Xi *et al.*, "Substantial global carbon uptake by cement carbonation," *Nat. Geosci.*,
412 vol. 9, no. 12, pp. 880–883, 2016.

413 [7] R. Zulcão, J. L. Calmon, T. A. Rebello, and D. R. Vieira, "Life cycle assessment of the
414 ornamental stone processing waste use in cement-based building materials," *Constr.*
415 *Build. Mater.*, vol. 257, p. 119523, 2020.

416 [8] H. Dada, A. S. E. Belaidi, H. Soualhi, E.-H. Kadri, and B. Benabed, "Influence of
417 temperature on the rheological behaviour of eco-mortar with binary and ternary
418 cementitious blends of natural pozzolana and marble powder," *Powder Technol.*, 2021.

419 [9] K. Wang, L. Du, X. Lv, Y. He, and X. Cui, "Preparation of drying powder inorganic
420 polymer cement based on alkali-activated slag technology," *Powder Technol.*, vol. 312,
421 pp. 204–209, 2017.

422 [10] G. J. B. Silva, V. P. Santana, and M. Wójcik, "Investigation on mechanical and
423 microstructural properties of alkali-activated materials made of wood biomass ash and
424 glass powder," *Powder Technol.*, vol. 377, pp. 900–912, 2021.

425 [11] J. L. Provis, "Alkali-activated materials," *Cem. Concr. Res.*, vol. 114, pp. 40–48, 2018.

426 [12] A. Hasnaoui, E. Ghorbel, and G. Wardeh, "Effect of Curing Conditions on the
427 Performance of Geopolymer Concrete Based on Granulated Blast Furnace Slag and
428 Metakaolin," *J. Mater. Civ. Eng.*, vol. 33, no. 3, p. 4020501, 2021.

429 [13] H. Ma, H. Zhu, C. Wu, H. Chen, J. Sun, and J. Liu, "Study on compressive strength
430 and durability of alkali-activated coal gangue-slag concrete and its mechanism,"
431 *Powder Technol.*, vol. 368, pp. 112–124, 2020.

432 [14] A. Autef *et al.*, "Role of metakaolin dehydroxylation in geopolymer synthesis,"

433 *Powder Technol.*, vol. 250, pp. 33–39, 2013.

434 [15] J. L. Provis, A. Palomo, and C. Shi, "Advances in understanding alkali-activated
435 materials," *Cem. Concr. Res.*, vol. 78, pp. 110–125, 2015.

436 [16] A. Hasnaoui, E. Ghorbel, and G. Wardeh, "Optimization approach of granulated blast
437 furnace slag and metakaolin based geopolymer mortars," *Constr. Build. Mater.*, vol.
438 198, pp. 10–26, 2019, doi: 10.1016/j.conbuildmat.2018.11.251.

439 [17] C. Ouellet-Plamondon and G. Habert, "Life cycle assessment (LCA) of alkali-activated
440 cements and concretes," in *Handbook of alkali-activated cements, mortars and*
441 *concretes*, Elsevier, 2015, pp. 663–686.

442 [18] A. Nazari and J. G. Sanjayan, *Handbook of low carbon concrete*. Butterworth-
443 Heinemann, 2016.

444 [19] B. Coppola, J.-M. Tulliani, P. Antonaci, and P. Palmero, "Role of Natural Stone
445 Wastes and Minerals in the Alkali Activation Process: A Review," *Materials (Basel).*,
446 vol. 13, no. 10, p. 2284, 2020.

447 [20] P. Perez-Cortes and J. I. Escalante-Garcia, "Alkali activated metakaolin with high
448 limestone contents–Statistical modeling of strength and environmental and cost
449 analyses," *Cem. Concr. Compos.*, vol. 106, p. 103450, 2020.

450 [21] D. E. Ortega-Zavala, J. L. Santana-Carrillo, O. Burciaga-Díaz, and J. I. Escalante-
451 García, "An initial study on alkali activated limestone binders," *Cem. Concr. Res.*, vol.
452 120, pp. 267–278, 2019.

453 [22] U. Avila-López, J. M. Almanza-Robles, and J. I. Escalante-García, "Investigation of
454 novel waste glass and limestone binders using statistical methods," *Constr. Build.*
455 *Mater.*, vol. 82, pp. 296–303, 2015.

[23] W. J. McNulty Jr, “Inorganic cementitious material.” Google Patents, Jul. 24, 2001.

[24] D. H. Nguyen, M. Boutouil, N. Sebaibi, F. Baraud, and L. Leleyter, “Durability of pervious concrete using crushed seashells,” *Constr. Build. Mater.*, vol. 135, pp. 137–150, 2017.

[25] U. G. Eziefula, J. C. Ezeh, and B. I. Eziefula, “Properties of seashell aggregate concrete: A review,” *Constr. Build. Mater.*, vol. 192, pp. 287–300, 2018.

[26] K. H. Mo, U. J. Alengaram, M. Z. Jumaat, S. C. Lee, W. I. Goh, and C. W. Yuen, “Recycling of seashell waste in concrete: A review,” *Constr. Build. Mater.*, vol. 162, pp. 751–764, 2018.

[27] Y. Zhang *et al.*, “Study on engineering properties of foam concrete containing waste seashell,” *Constr. Build. Mater.*, vol. 260, p. 119896, 2020.

[28] D. H. Nguyen, M. Boutouil, N. Sebaibi, L. Leleyter, and F. Baraud, “Valorization of seashell by-products in pervious concrete pavers,” *Constr. Build. Mater.*, vol. 49, pp. 151–160, 2013.

[29] B. Safi, M. Saidi, A. Daoui, A. Bellal, A. Mechekak, and K. Toumi, “The use of seashells as a fine aggregate (by sand substitution) in self-compacting mortar (SCM),” *Constr. Build. Mater.*, vol. 78, pp. 430–438, 2015.

[30] G. Caglioti, A. t Paoletti, and F. P. Ricci, “Choice of collimators for a crystal spectrometer for neutron diffraction,” *Nucl. Instruments*, vol. 3, no. 4, pp. 223–228, 1958.

[31] S. Gražulis *et al.*, “Crystallography Open Database (COD): an open-access collection of crystal structures and platform for world-wide collaboration,” *Nucleic Acids Res.*, vol. 40, no. D1, pp. D420–D427, 2012.

[32] L. Lutterotti, S. Matthies, H.-R. Wenk, A. S. Schultz, and J. W. Richardson Jr, "Combined texture and structure analysis of deformed limestone from time-of-flight neutron diffraction spectra," *J. Appl. Phys.*, vol. 81, no. 2, pp. 594–600, 1997.

[33] M. S. Kim, Y. Jun, C. Lee, and J. E. Oh, "Use of CaO as an activator for producing a price-competitive non-cement structural binder using ground granulated blast furnace slag," *Cem. Concr. Res.*, vol. 54, pp. 208–214, 2013.

[34] W. Deboucha, N. Leklou, A. Khelidj, and M. N. Oudjit, "Hydration development of mineral additives blended cement using thermogravimetric analysis (TGA): Methodology of calculating the degree of hydration," *Constr. Build. Mater.*, vol. 146, pp. 687–701, 2017.

[35] D. R. Johnson and W. A. Robb, "Gaylussite: thermal properties by simultaneous thermal analysis," *Am. Mineral. J. Earth Planet. Mater.*, vol. 58, no. 7–8, pp. 778–784, 1973.

[36] A. Navrotsky, R. L. Putnam, C. Winbo, and E. Rosén, "Thermochemistry of double carbonates in the K2 CO3-CaCO3 system," *Am. Mineral.*, vol. 82, no. 5–6, pp. 546–548, 1997.

[37] W. U. Malik, D. R. Gupta, I. Masood, and R. S. Gupta, "Kinetic study of thermal decomposition of calcium carbonate in the presence of K 2 CO 3 and BaCO 3," *J. Mater. Sci. Lett.*, vol. 4, no. 5, pp. 532–536, 1985.

[38] G. Anbalagan, P. Rajakumar, and S. Gunasekaran, "Non-isothermal decomposition of Indian limestone of marine origin," *J. Therm. Anal. Calorim.*, vol. 97, no. 3, pp. 917–921, 2009.

[39] R. Subasri and H. Näfe, "Phase evolution on heat treatment of sodium silicate water

glass," *J. Non. Cryst. Solids*, vol. 354, no. 10–11, pp. 896–900, 2008.

[40] A. Bloise *et al.*, "TG/DSC study of the thermal behaviour of hazardous mineral fibres," *J. Therm. Anal. Calorim.*, vol. 123, no. 3, pp. 2225–2239, 2016.

[41] M. Frías, R. V. De La Villa, R. Garcia, S. Martínez-Ramírez, and L. Fernández-Carrasco, "New developments in low clinker cement paste mineralogy," *Appl. Clay Sci.*, vol. 166, pp. 94–101, 2018.

[42] P. Yu, R. J. Kirkpatrick, B. Poe, P. F. McMillan, and X. Cong, "Structure of calcium silicate hydrate (C-S-H): Near-, Mid-, and Far-infrared spectroscopy," *J. Am. Ceram. Soc.*, vol. 82, no. 3, pp. 742–748, 1999.

[43] I. G. Lodeiro, D. E. Macphee, A. Palomo, and A. Fernández-Jiménez, "Effect of alkalis on fresh C–S–H gels. FTIR analysis," *Cem. Concr. Res.*, vol. 39, no. 3, pp. 147–153, 2009.

[44] E. Ferraz, J. A. F. Gamelas, J. Coroado, C. Monteiro, and F. Rocha, "Recycling waste seashells to produce calcitic lime: characterization and wet slaking reactivity," *Waste and biomass valorization*, vol. 10, no. 8, pp. 2397–2414, 2019.

[45] S. Gunasekaran, G. Anbalagan, and S. Pandi, "Raman and infrared spectra of carbonates of calcite structure," *J. Raman Spectrosc. An Int. J. Orig. Work all Asp. Raman Spectrosc. Incl. High. Order Process. also Brillouin Rayleigh Scatt.*, vol. 37, no. 9, pp. 892–899, 2006.

[46] F. Farcas and P. Touze, "La spectrométrie infrarouge à transformée de Fourier (IRTF)," *Une méthode intéressante pour la caractérisation des ciments (in French) Bull. Lab. Ponts Chaussées*, vol. 230, pp. 77–88, 2001.

[47] M. Trivedi, A. Branton, D. Trivedi, H. Shettigar, K. Bairwa, and S. Jana, "Fourier

transform infrared and ultraviolet-visible spectroscopic characterization of biofield treated salicylic acid and sparfloxacin," *Nat. Prod. Chem. Res.*, vol. 5, no. 3, 2015.

[48] E. G. Krukowski, A. Goodman, G. Rother, E. S. Ilton, G. Guthrie, and R. J. Bodnar, "FT-IR study of CO2 interaction with Na+ exchanged montmorillonite," *Appl. Clay Sci.*, vol. 114, pp. 61–68, 2015.

[49] P. A. Gerakines, W. A. Schutte, J. M. Greenberg, and E. F. van Dishoeck, "The infrared band strengths of H2O, CO and CO2 in laboratory simulations of astrophysical ice mixtures," *arXiv Prepr. astro-ph/9409076*, 1994.

[50] F. Puertas, S. Martínez-Ramírez, S. Alonso, and T. Vazquez, "Alkali-activated fly ash/slag cements: strength behaviour and hydration products," *Cem. Concr. Res.*, vol. 30, no. 10, pp. 1625–1632, 2000.

## List of figures

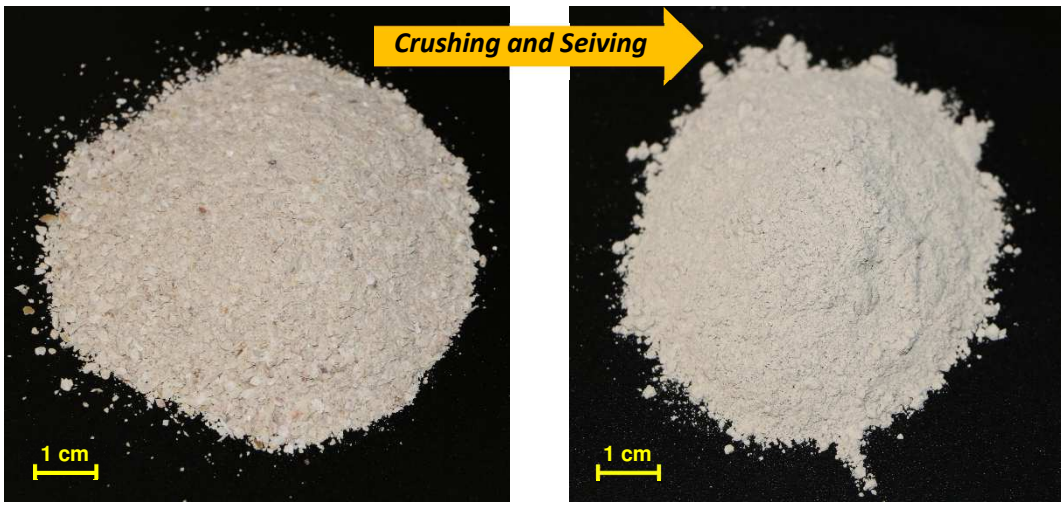


**Fig. 1**. Preparation of SW powder (b) by crushing SW aggregate (a) and seiving the obtained powder with 63 µm seive.

21

22

23

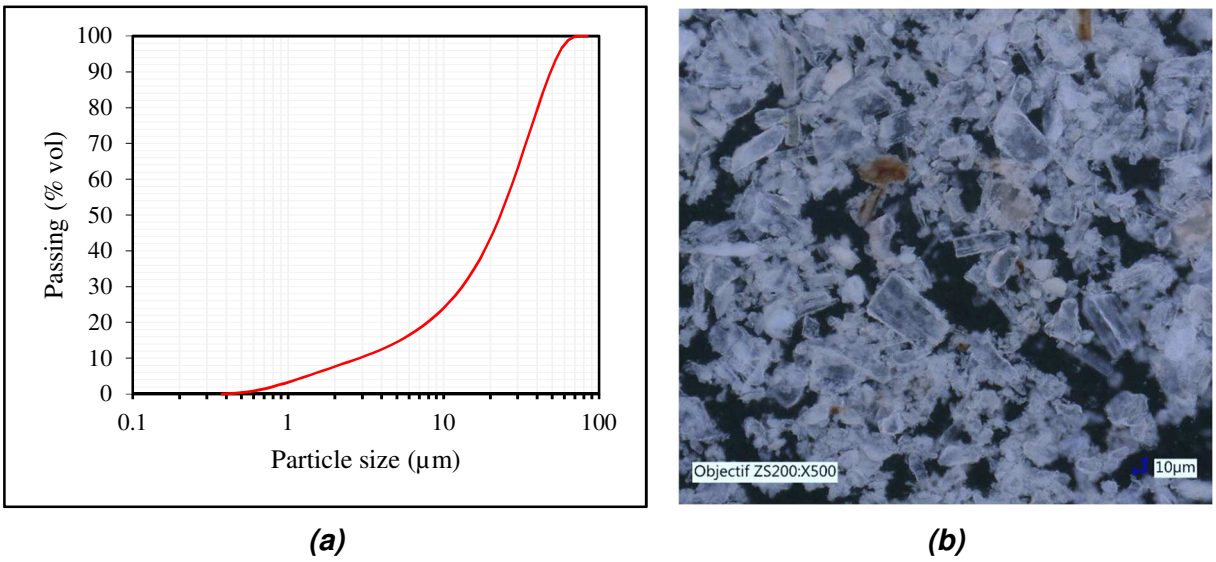


**Fig. 2**. Particle size distribution (a) of SW powder and its particle morphology from optical microscope (b).

24

25

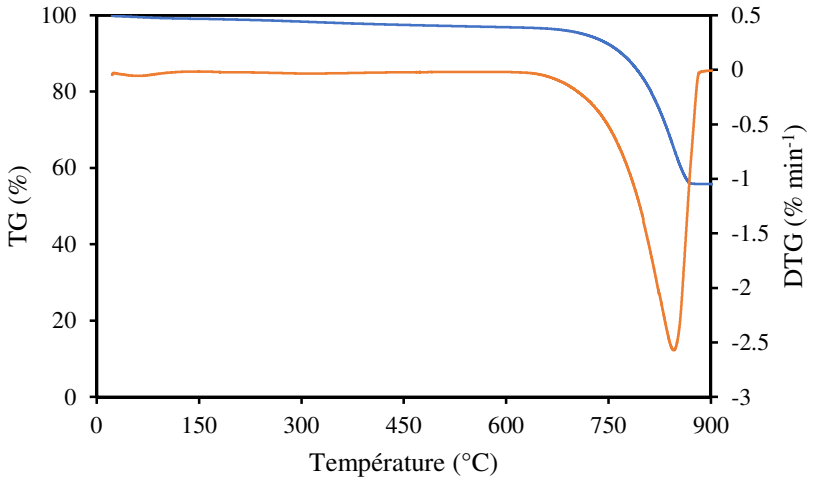


**Fig. 3**. Thermal gravimetric analysis of SW powder.

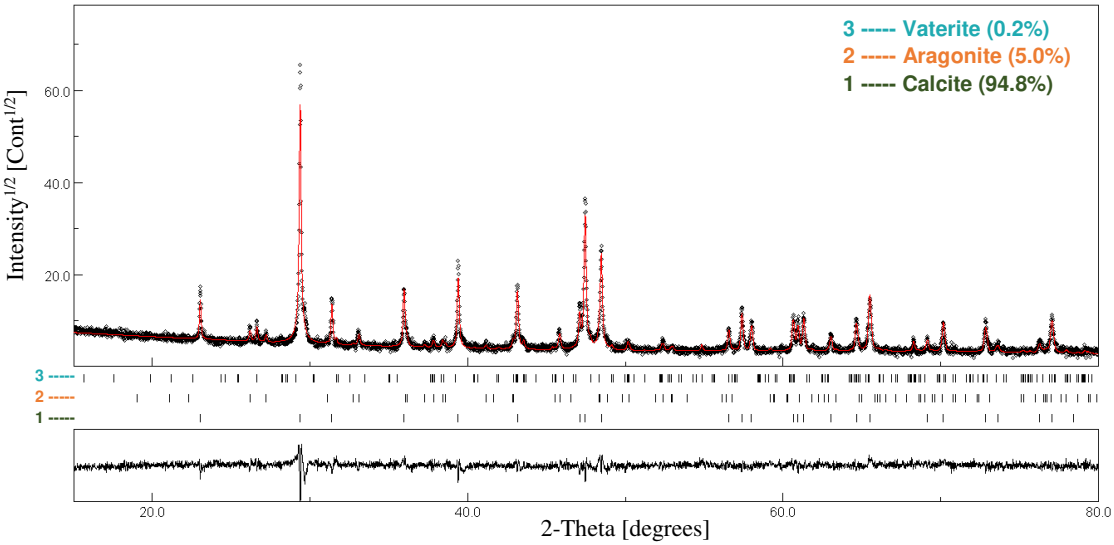


**Fig. 4**. XRD pattern of SW powder.

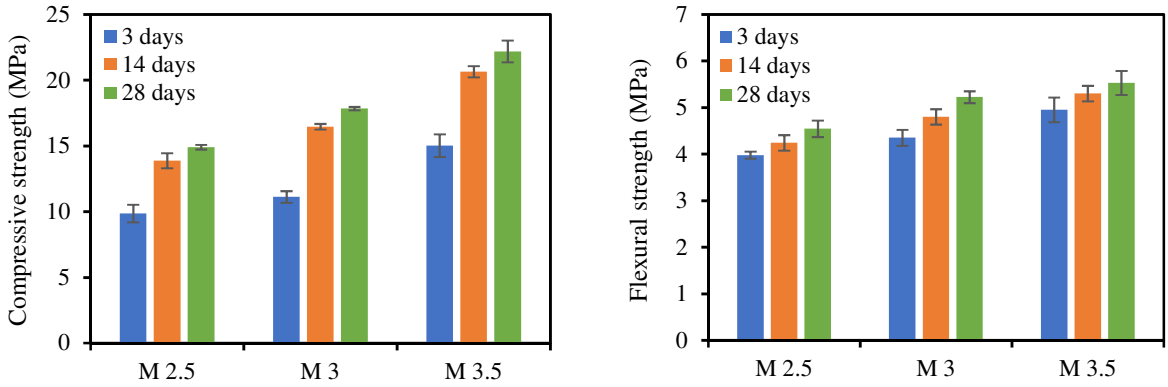


**Fig. 5**. Mechanical strengths evolution of AASW mortars.

32

33

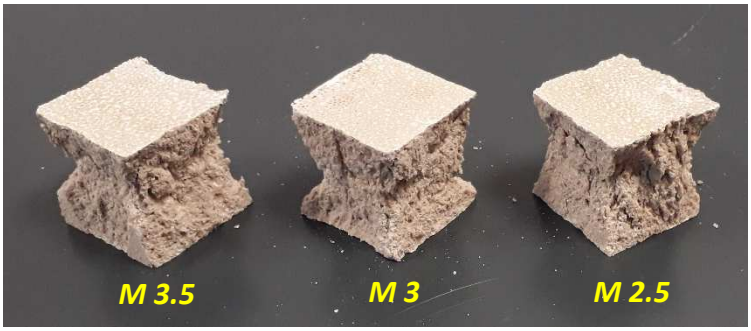


**Fig. 6**. Failure pattern of AASW mortars under uniaxial compression test at 28 days.

34

35

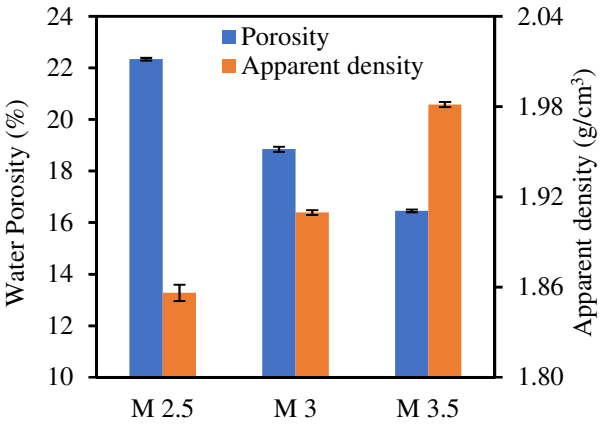


**Fig. 7**. Water porosity and apparent density of AASW mortars.

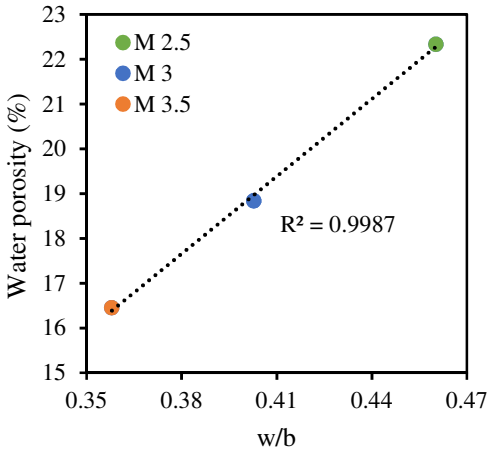


**Fig. 8**. Water porosity of AASW mortars versus w/b ratio.

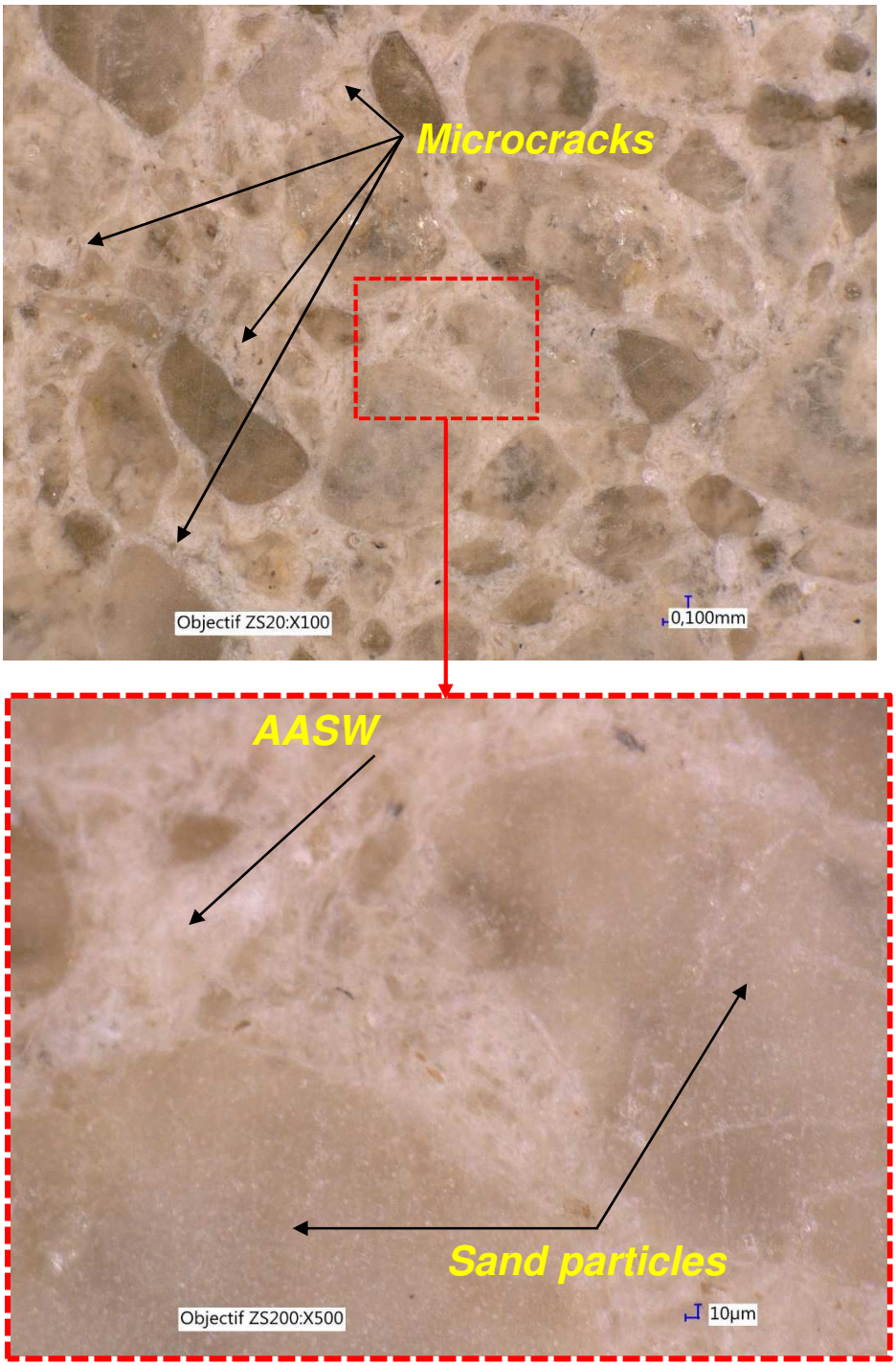


**Fig. 9**. Optical microscope images of M 3.5.

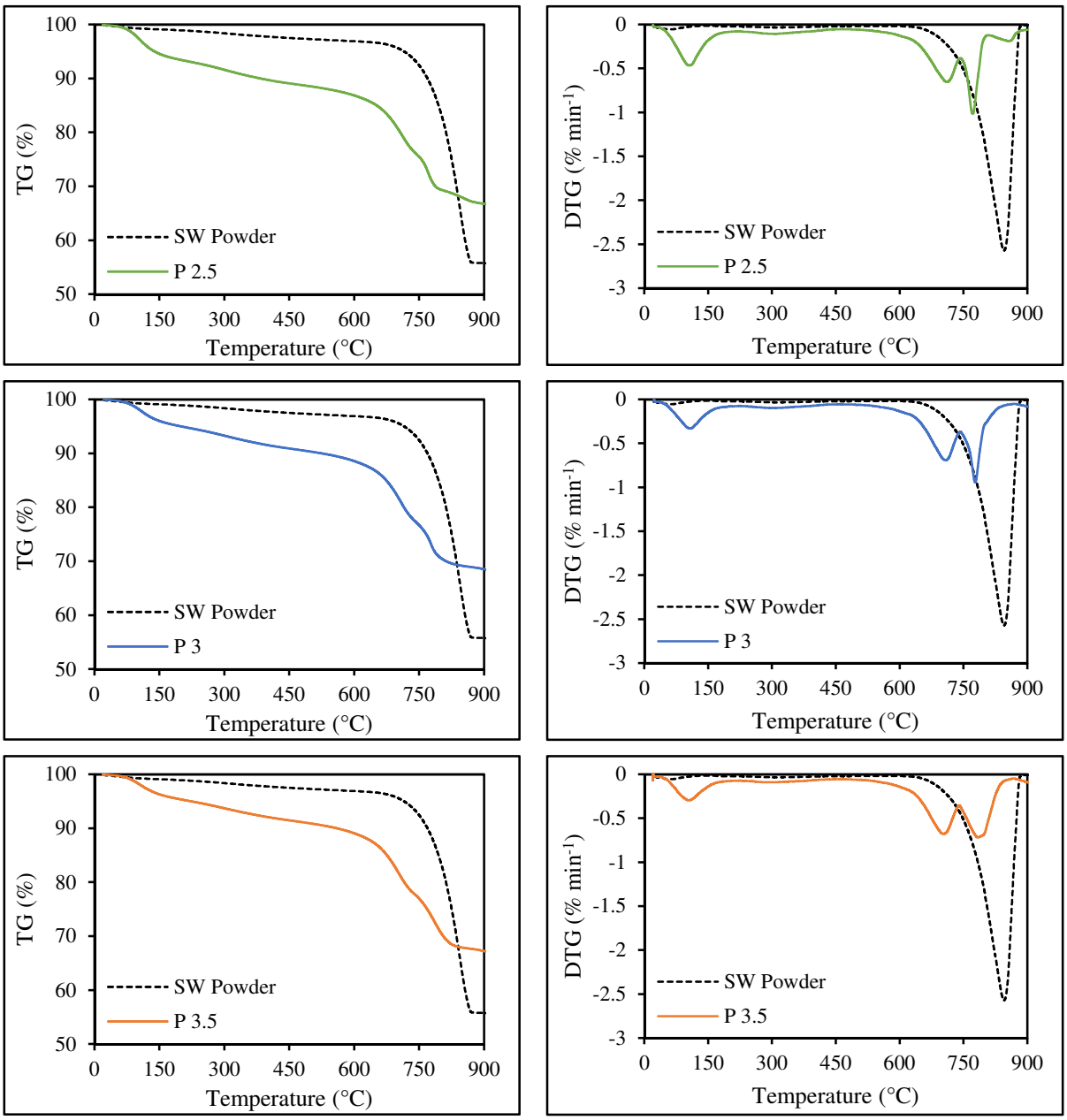


**Fig. 10**. TG/DTG curves of AASW pastes at 28 days.

42

43

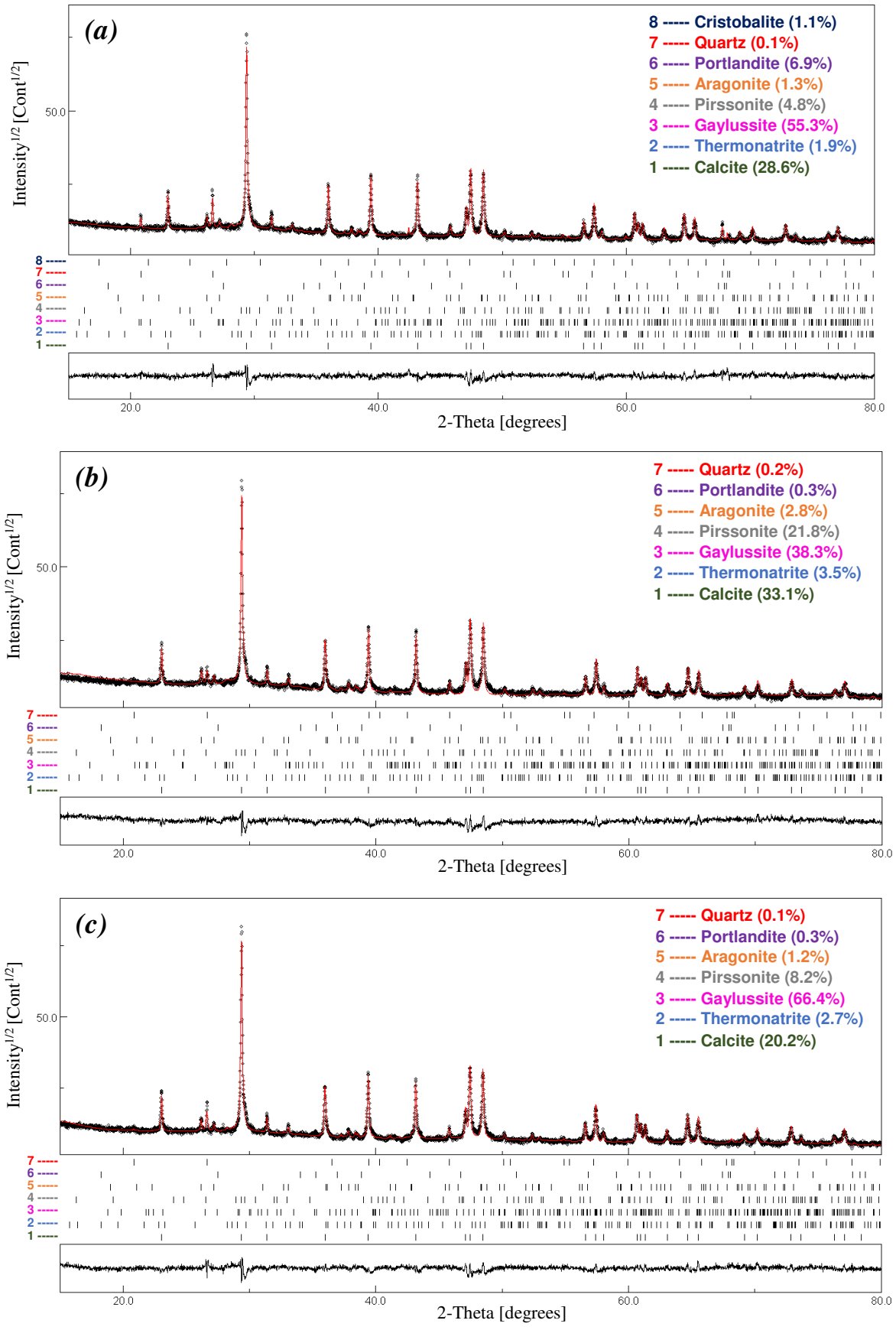


**Fig. 11**. XRD patterns of AASW pastes: (a) P 2.5, (b) P 3 and (c) P 3.5.

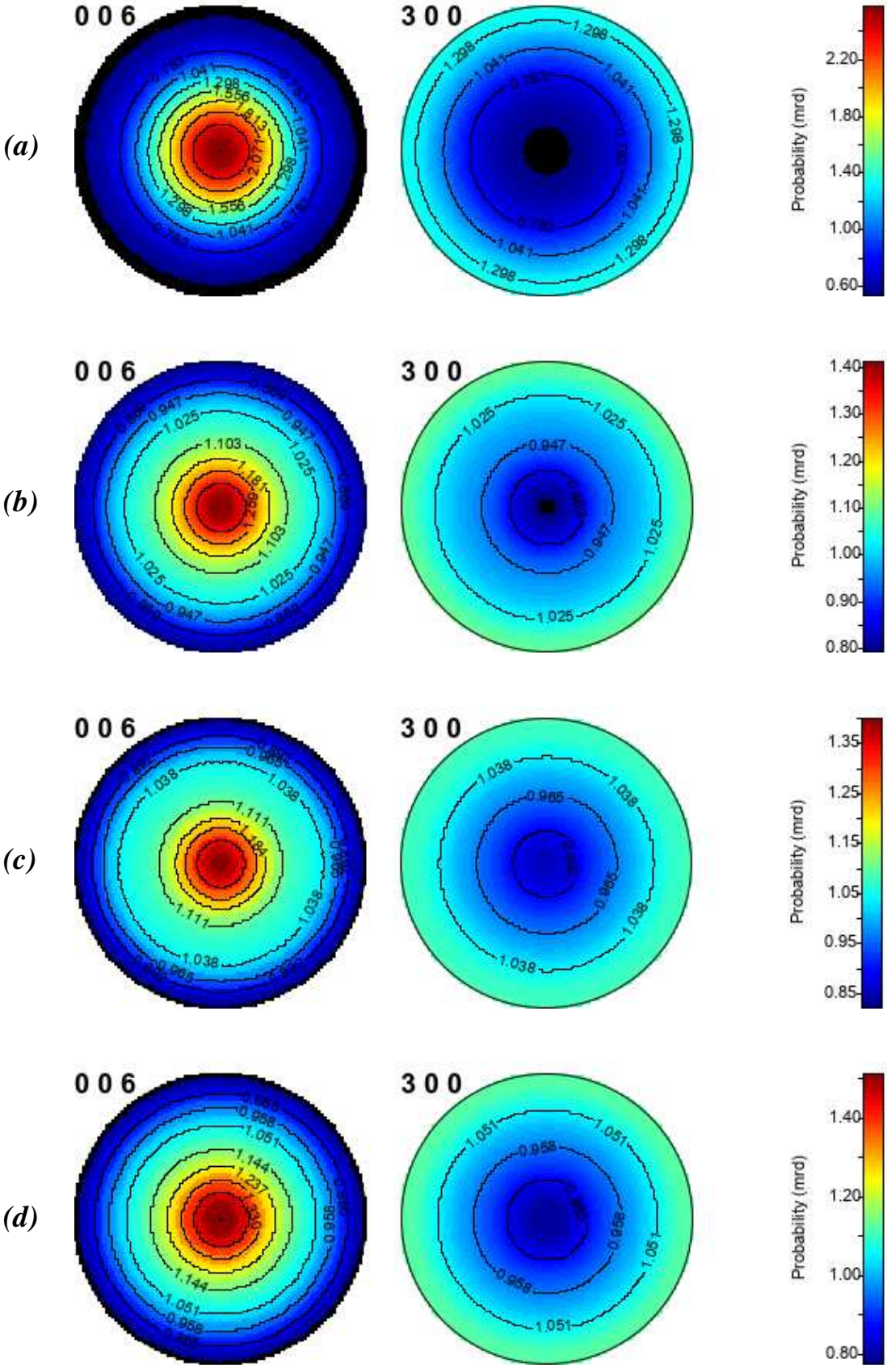


**Fig. 12**. Pole figures of calcite: *(a)* SW Powder, *(b)* P 2.5, *(c)* P 3 and *(d)* P 3.5.

45

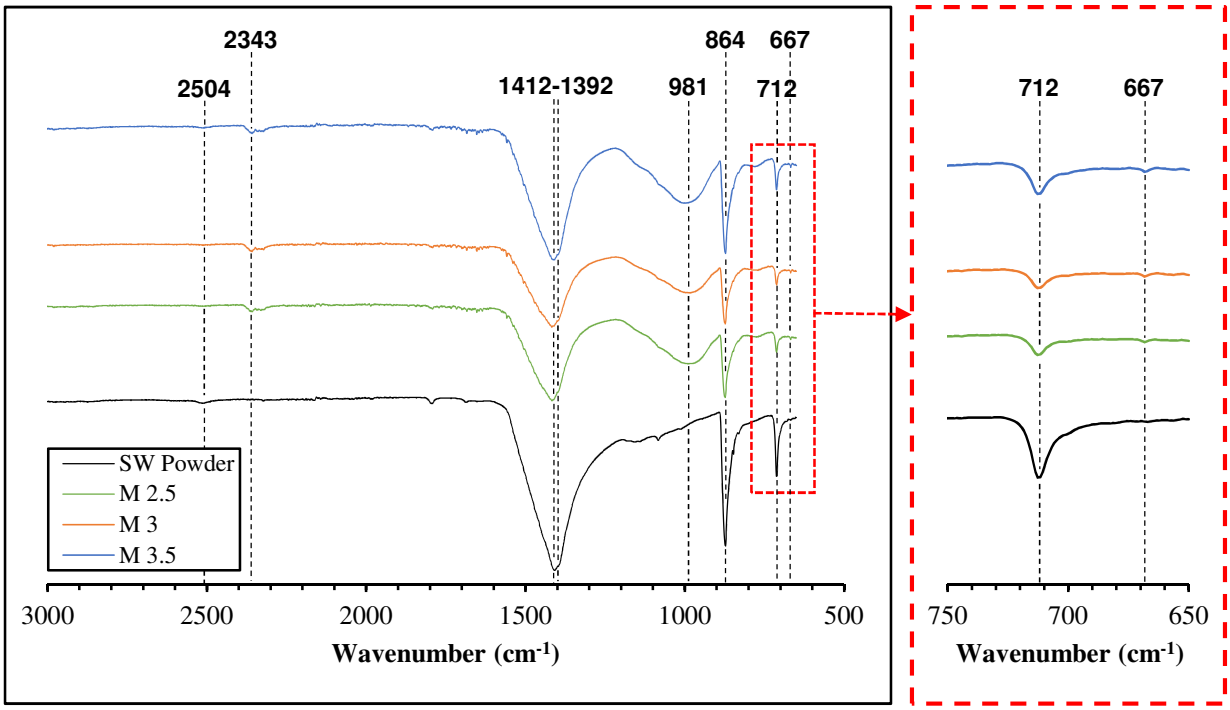


**Fig. 13**. FTIR spectra of SW powder and AASW pastes at 28 days.

46

## List of tables



**Table 1**. Chemical composition of SW powder.

| **Chemical elements** | **g.kg$^{-1}$** |
|---|---|
| Ca | $368^{\pm 5}$ |
| S | $6.80^{\pm 0.2}$ |
| Na | $3.90^{\pm 0.1}$ |
| Mg | $1.10^{\pm 0.1}$ |
| Fe | $0.80^{\pm 0.09}$ |
| Sr | $0.68^{\pm 0.02}$ |
| K | $0.33^{\pm 0.04}$ |
| Al | $0.26^{\pm 0.06}$ |
| Ni | $0.07^{\pm 0.01}$ |
| Mn | $0.018^{\pm 0.002}$ |

**Table 2**. Chemical composition of SS.

| | $SiO_2$ (%wt.) | $Na_2O$ (%wt.) | $H_2O$ (%wt.) |
|---|---|---|---|
| **Sodium silicate** ($Na_2SiO_3$) | 25.5 | 12.8 | 61.7 |

21 **Table 3**. Mix proportions of alkali activated SW mortars and pastes.

| Samples type | Mixtures | MR | $\frac{SW}{Activator}$ | SW (g) | Sand (g) | SS (g) | w/b* | Flow (mm) |
|---|---|---|---|---|---|---|---|---|
| Mortars | M 2.5 | 2.1 | 2.5 | 450 | 1350 | 470 | 0.46 | 157 |
| | M 3 | | 3 | | | 392 | 0.40 | 123 |
| | M 3.5 | | 3.5 | | | 336 | 0.36 | 108 |
| Pastes | P 2.5 | 2.1 | 2.5 | 450 | - | 470 | 0.46 | - |
| | P 3 | | 3 | | | 392 | 0.40 | |
| | P 3.5 | | 3.5 | | | 336 | 0.36 | |

22 *b: total weight of SW powder and the dry extract of SS (Activator).

23

24

25 **Table 4**. Absorption bands obtained for SW powder and AASW pastes along with their
26 assignment.

| Spectral position | Assignment | References |
|---|---|---|
| 667 $cm^{-1}$ | δ Si-O-Si | [16], [45] |
| 712 $cm^{-1}$ | $\nu_4$ C-O ($CO_3^{2-}$) | [39], [40] |
| 864 $cm^{-1}$ | $\nu_2$ C-O ($CO_3^{2-}$) | [39], [41] |
| 981 $cm^{-1}$ | ν Si-O (C-S-H) | [16], [36]–[38] |
| 1392 $cm^{-1}$ | $\nu_3$ C-O ($CO_3^{2-}$) | [39] |
| 1412 $cm^{-1}$ | $\nu_3$ C-O ($CO_3^{2-}$) | [38], [39], [42] |
| 2343 $cm^{-1}$ | $\nu_3$ C-O ($CO_2$) | [43], [44] |
| 2504 $cm^{-1}$ | $2\nu_2 + \nu_4$ C-O ($CO_3^{2-}$) | [39] |

27

## Graphical abstract